Action Plots in Action: In-Depth Insights into Photochemical Reactivity

Ishrath Mohamed Irshadeen,[‖] Sarah L. Walden,[‖] Martin Wegener, Vinh X. Truong,* Hendrik Frisch,* James P. Blinco,* and Christopher Barner-Kowollik*

ABSTRACT: Predicting wavelength-dependent photochemical reactivity is challenging. Herein, we revive the well-established tool of measuring action spectra and adapt the technique to map wavelength-resolved covalent bond formation and cleavage in what we term "photochemical action plots". Underpinned by tunable lasers, which allow excitation of molecules with near-perfect wavelength precision, the photoinduced reactivity of several reaction classes have been mapped in detail. These include photoinduced cycloadditions and bond formation based on photochemically generated *o*-quinodimethanes and 1,3-dipoles such as nitrile imines as well as radical photoinitiator cleavage. Organized by reaction class, these data demonstrate that UV/vis spectra fail to act as a predictor for photochemical reactivity at a given wavelength in most of the examined reactions, with the photochemical reactivity being strongly red shifted in comparison to the absorption spectrum. We provide an encompassing perspective of the power of photochemical action plots for bond-forming reactions and their emerging applications in the design of wavelength-selective photoresists and photoresponsive soft-matter materials.

INTRODUCTION

Photochemistry is perhaps the most far-reaching, impactful, and enabling of all chemical processes,[1] given that life on Earth itself is sustained by photosynthesis enabled by the energy of sunlight.[2] In human endeavors, photochemical processes have been used since antiquity to cure materials. The literature on photochemical processes is vast and diverse and has experienced a significant increase with the advent of laser technology. The commercial availability of tunable laser systems has enabled the ability to finely adjust not only the intensity of light but more importantly its wavelength.[3]

Photochemists have long sought to identify which color of light will afford the most effective reaction pathway to the desired product. On the simplest level, the absorption spectrum of a molecule provides guidance on the most effective electronic transitions, which are often portrayed in a Jablonski diagram.[4] It is also possible to computationally determine the absorption spectrum via quantum chemical methods, such as density functional theory (DFT), to gain an understanding of its structure before any synthetic effort is undertaken. However, knowledge of the absorption spectrum alone has been shown to be insufficient to predict the wavelength at which photochemical reaction channels can be activated most effectively.[5] This is perhaps most prominent in anti-Kasha molecules, where the first electronic transition is chemically inactive.[6]

Modern soft-matter materials science and polymer chemistry provide the chemical foundations for a wide range of photoactive materials.[7] These materials include surface coatings, medical materials and 3D printing photoresists (reaction mixtures that can be solidified by light).[8] Classically, these photoresists have been cured with a specific color of light (or a narrow range of colors emitted from an LED or in some cases with very broad emitting light sources), yielding one specific material property.[9] Recently, photoresist technology has moved into a new phase, in which multicomponent mixtures contain unique reactive chromophores that are responsive to a specific color of light, enabling multimaterial 3D printing from a single resist (or from the user's point of view, a single printer cartridge).[10] In a projection forward into the future, the user of a 3D printer would select not only the printed geometry but also a specific material property that is to be printed at a specific location within the structure. The technology could include such disparate materials properties as conducting vs insulating or degradable vs nondegradable components. To achieve such a selective photoresist, near-perfect wavelength orthogonality (sometimes also referred to as chromatic orthogonality or chromatic selectivity)[11] between the photoreactive groups is a prerequisite.[12] It is pivotal that the activation of the chromophores occurs independently of the sequence in which the different colors of light are applied, which is a tall order. To achieve such a high level of orthogonality, it is imperative to have information on the wavelength-resolved reactivity for each photoreactive system in the solution, relative to their absorption spectrum in the same solvent. Such information is provided by photochemical action plots, which have experienced a renaissance over the last 6

Scheme 1. Evolution of Action Plot Technology from Photobiological Action Spectra (Panel 1, Top Left) to the Finely Resolved Wavelength Mapping of Covalent Reactions of Distinct Molecules (Panel 2, Top Right)[a]

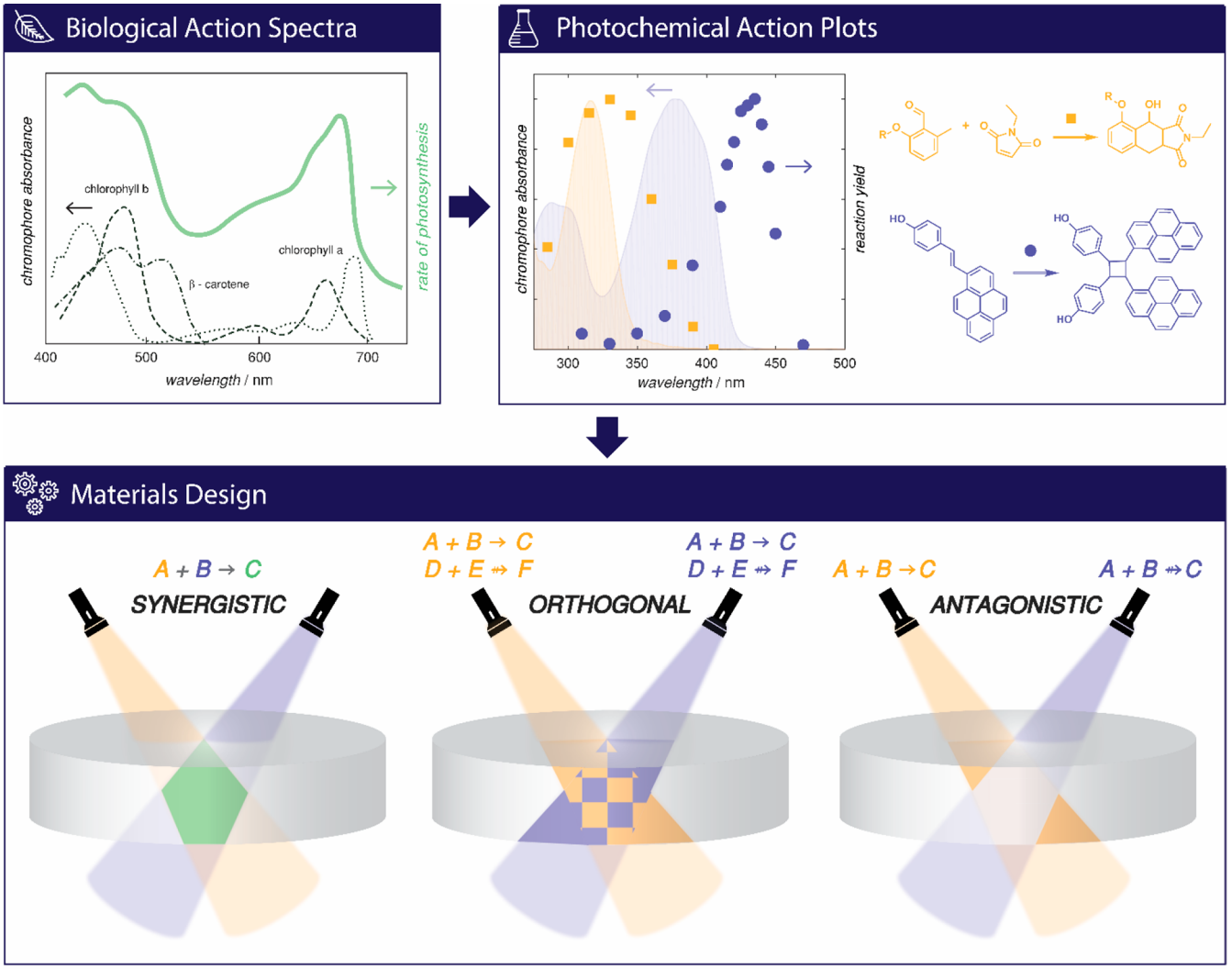

[a]The information gained from action plots forms the basis for wavelength-gated sets of reactions in a (soft matter) materials science context. Such reaction systems include synergistic photoreactions that only occur in the presence of two distinct wavelengths (bottom left), orthogonal systems where specific wavelengths initiate exclusively one reaction without affecting another (bottom middle), and antagonistic systems, where two wavelengths are required to suppress a reaction (bottom right).

years, driven by the emerging field of light-driven one- and two-photon activated 3D printing.

The current Perspective surveys the state of the art in photochemical action plots and projects a path forward for the wavelength-gated design of functional materials, empowered by photochemical reaction systems that operate synergistically, orthogonally, or antagonistically (Scheme 1).

BACKGROUND

The idea of measuring wavelength-dependent chemical activity is, of course, not a new one. Studies to date have primarily focused on three broad fields: biological activity, photovoltaics, and photodissociation.

Since the late 19th century, intense research has been undertaken to understand the different biological responses to specific wavelengths. The vast majority of these studies utilize broad-band lamps with narrow filters to assess the photodamage resulting from solar radiation. The effect of irradiation has been quantified by metrics such as cell viability,[13] vitamin D3 degradation,[14,15] production of erythema,[16] changes in DNA,[17−19] and the appearance of tumors,[20] just to name a few. A critical evaluation of the active wavelength regions of the mechanism studied can be used to identify the contributing chromophore leading to such processes. We consider here the well-studied action of photosynthesis (Scheme 1, panel 1). There are several key chromophores that contribute to the absorption of solar radiation in plants and other biological materials (black lines). Since these chromophores are instrumental in converting solar energy to chemical energy driving photosynthesis, it is unsurprising that the net absorption of these chromophores closely matches the wavelength-dependent rate of photosynthesis (green line), usually determined by monitoring oxygen production or carbon fixation. It was the correlation between these two curves that led to the discovery of chlorophyll as the key chromophore for plant growth.[21] This has been possible based on the basis of the assumption that the absorbance spectrum of the chromophore closely matches the action spectrum. The

importance of studies such as these cannot be underestimated, as they have been instrumental in identifying DNA as the core genetic material[22] revealing the key wavelengths leading to skin cancer,[23] the transparent optical window of biological tissue[24] and the role of color in influencing circadian rhythms.[25] Several reviews have been written on the topic, and thus they will not be the focus of the current Perspective.[26,27]

The late 20th century saw a rise in the development of optical devices capable of harvesting sunlight efficiently for applications such as photocatalysis[28] and photovoltaics.[29] Here, action spectra became routine measurements to determine the photocurrent efficiency at various wavelengths, typically achieved using broad-band lamps coupled to a diffraction grating. The information obtained from these studies has been vital in understanding the primary contributors to photocurrent generation[30,31] in order to develop new materials,[32−34] morphologies[35,36] and device designs[37−39] to enhance the capture and utilization of solar energy.

Within the field of photochemistry, action spectra have been primarily limited to photodissociation studies, where a monochromatic light source, usually a laser, is coupled to a mass spectrometer and the wavelength-dependent dissociation of ions in the gaseous phase is recorded.[40] As with biological studies, photodissociation action spectra have been utilized to identify the contributing chromophore in molecular systems,[41,42] in addition to characterizing radical generation and unstable isomers[43−45] and understanding higher state electron dynamics.[46,47]

The above is of course not an exhaustive list, and other wavelength-dependent chemical studies have covered broad areas in polymer degradation,[48] surface characterization,[49] and phototherapy.[50] While these studies have been vital in broadening our understanding of chemical processes and bond strengths, they have primarily focused on bond-breaking and isomerization mechanisms. In contrast, herein we highlight the body of work conducted in characterizing wavelength-dependent control over bond formation for advanced material design using different colors of light.

METHODOLOGY

"Action plots", as outlined in the current Perspective, were rejuvenated and refined as a critical tool to assess photochemical covalent bond formation approximately 6 years ago, by our team. The most influential factor behind this resurgence is the affordable availability of optical parametric oscillators (OPOs), which are tunable nanosecond pulsed lasers capable of emitting monochromatic light across a broad range of wavelengths from the deep-UV to near-infrared. In comparison to broad-band light sources, such as LEDs or lamps equipped with either a diffraction grating or filters (which both severely limit the light intensity and are never truly monochromatic), the implementation of tunable lasers in photochemistry has allowed the intensity, as well as the wavelength, of light to be precisely tuned according to the users' needs. This prompted the concept of mapping chemical activity against wavelength to be revisited with renewed focus.

The experimental method of acquiring an action plot via a tunable laser has been included in detail in the Supporting Information as a tutorial to any user who wishes to conduct such experiments. Briefly, an identical batch of samples is prepared at a suitable concentration to minimize light attenuation throughout the sample volume, while maintaining sufficient material for characterization. Each sample is irradiated with an identical number of photons of monochromatic light across the wavelength region of interest. Irradiation is followed by careful quantitative characterization to determine the yield of the reaction. The characterization method will vary depending on the chemical system and concentrations used. Ideally, structural methods such as NMR spectroscopy or mass spectrometry, coupled to a suitable separatory method (LC-MS or SEC-MS), should be used for quantification. However, the concentrations required for these techniques are not always practical. Therefore, indirect methods, such as absorbance and fluorescence, can be employed if the optical properties allow. The error in these measurements will vary depending on the chosen characterization method but can be minimized by performing measurements at each wavelength in triplicate.

Once the wavelength-dependent reactivity has been elucidated, a graph is prepared by overlaying the reactivity with the molar extinction spectrum, measured in the reaction solvent. An example of such a plot for two different photochemical systems is presented in Scheme 1, panel 2, where the dots indicate the reaction conversion and the shaded areas indicate the absorbance spectra.

It is important to note here that what is often measured for optical characterization of chromophores is the molar extinction spectrum. However, the extinction spectrum is not necessarily congruent with the absorption spectrum due to effects such as scattering and reflection. This deviation becomes particularly significant when the size of the optical system under investigation approaches the wavelength of the irradiation source.[51] For small-molecule systems, scattering cross sections are on the order of 10^{-25} cm^2 $molecule^{-1}$ and therefore the deviation between absorption and extinction is minimal.[52] For larger polymeric systems, these deviations should be considered.

DISCUSSION

All of the reactions explored so far largely fall into three categories: photocycloadditions, photothermal hybrid reactions, and photorelease (Norrish type) reactions. Some reactions, the reader may find, can fall into more than one category. We have discussed those reactions in the section we judged as most appropriate but have included a discussion on any classification overlaps that we noticed. For ease of comparison, action plot data obtained within each reaction class have been normalized by the number of molecules in solution and the number of photons delivered during irradiation (refer to section 2 in the Supporting Information), and are reported as "adjusted % yields". For the sake of clarity, error ranges have not been represented on these graphs but can be found in the relevant literature. Typical error values are on the order of 3−5%. Where available, molar extinction coefficients have been provided. In cases where these were not reported, normalized absorbance spectra are provided instead.

Photocycloadditions. Photocycloadditions are among the oldest photoreactions in the field of synthetic chemistry. The [4 + 4] photocycloaddition of anthracene was first described by Fritzsche in 1867[53] and still finds ample application in chemistry due to its selectivity and catalyst-free nature.[54−57] Despite a plethora of research exploring photocycloadditions, almost all applications in photoligations utilize harsh UV light to initiate anthracene photodimerization. Only recently, we began to investigate the wavelength (λ) dependence of

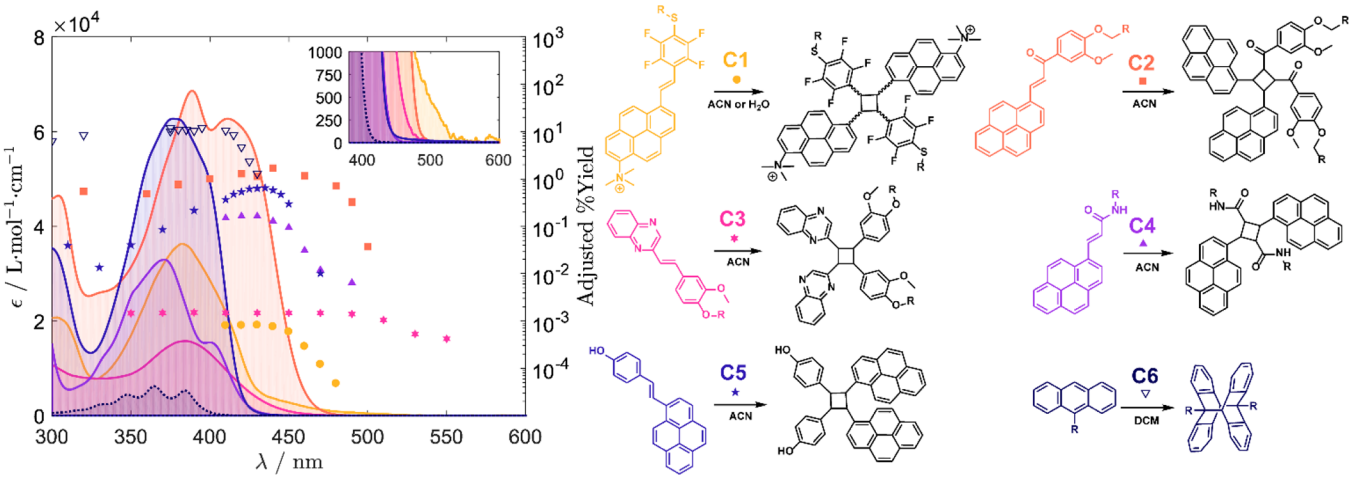

Figure 1. Molar extinction spectra (solid curves, left axis) and adjusted action plot yields (symbols, right axis) of various photocycloaddition reactions. For ease of comparison, percentage yields were adapted from the literature[58,59,62,67] and normalized by the number of photoreactive units in solution and the number of photons delivered to the sample to give adjusted % yields. The inset highlights the low-intensity absorption region. For the full methodology to arrive at the displayed action plots, refer to the Supporting Information.

anthracene photocycloaddition (Figure 1, reaction **C6**) using action plots.[58,59] Surprisingly, the reaction is initiated just as efficiently with visible light (λ = 410 nm) as with UV light (λ < 400 nm), challenging a paradigm of more than 100 years. We observed that the wavelength-dependent cycloaddition yield only decreases significantly at λ > 420 nm, where the extinction coefficient approaches zero, and at λ < 320 nm, where the competing photocycloreversion was observed to be highly efficient (Figure S4 in the Supporting Information).

In the realm of [2 + 2] photocycloadditions, the active development of red-shifted stilbene derivatives emerged after the rediscovery of styrylpyrene by the team of Asanuma.[60] As a side note, styrylpyrene was reported by Kovalenko and co-workers in 1980[61] yet only found application in 2016 as a visible-light-activated photoligation tool for the cross-linking of DNA strands.[60] To utilize the mildest possible activation wavelengths of styrylpyrene, we recorded an action plot of its photocycloaddition and photocycloreversion.[63] Surprisingly, the reactivity maximum of *trans*-(*p*-hydroxy)styrylpyrene (λ = 435 nm) was red-shifted by close to 60 nm in wavelength in comparison to the absorption maximum and the reactivity extends up to λ < 470 nm (Figure 1, **C5**). Moreover, the reactivity strongly decreased toward shorter wavelengths with a reactivity minimum at around λ = 330 nm. Since the action plot of the competing photocycloreversion of the styrylpyrene cycloadduct also displayed its reactivity maximum at λ = 330 nm, it is likely that the strongly decreased yield of the photocycloaddition at lower wavelengths results from the competing cycloreversion (Figure S3 in the Supporting Information).

The presence of such a low wavelength reactivity gap opens up key opportunities for the design of remotely controlled multireaction systems. In most cases, even mixtures of two photoreactive species of significantly different extinction maxima still display absorption overlaps at shorter wavelengths.[68] As a result, it is usually only possible to address the longer wavelength reactive species selectively, whereas irradiation with shorter wavelengths initiates both reactions at least partially. The experimental observation of a photochemical reactivity gap for styrylpyrene provided the foundation for the first chemical ligation system, where either one of the two reactions can be initiated exclusively as a function of wavelength (a concept termed sequence-independent λ-orthogonality).[10−12] If the kinetics of competing photocycloaddition and photocycloreversion are altered, for instance through tethering styrylpyrene units onto a polymer backbone, the strongly concentration dependent cycloaddition becomes more favored as the photoreactive moieties remain in close proximity after cycloreversion.[62] As a result, action plots of the styrylpyrene photocycloaddition in such a polymer-tethered scenario display a high reactivity in the UV range and the reactivity minimum around λ = 330 nm disappears.[62] Importantly, neither UV−vis absorbance nor fluorescence spectra displayed a significant change between *trans*-(*p*-hydroxy)styrylpyrene and its polymer-tethered counterpart, whereas the action plot directly revealed the altered wavelength-dependent reactivity.

To shift the activation wavelengths of [2 + 2] photocycloadditions further into the visible light, several stilbene derivatives with extended conjugated systems, and electron-withdrawing and -donating substituents, were synthesized and analyzed. Introducing a quaternized ammonium group as a pyrene substituent increased the charge-promoted water solubility and enhanced the triplet state (T_1) formation upon excitation. Concurrent perfluoration of the phenyl ring yielded 1-trimethylammonium-6-pentafluorostyrylpyrene (qStyPy).[69] A subsequent metal-free *p*-fluoro-thiol reaction gave rise to functionalized qStyPy-thioethers (R−qStyPy), which led to a further absorbance red shift of close to 14 nm to λ_{max} = 388 nm. In this case, the absorption red shift was concomitant with a red shift in reactivity up to λ > 480 nm, in comparison to styrylpyrene (Figure 1, **C1**). When the phenyl ring of styrylpyrene is substituted with an amide to obtain acrylamidylpyrene, a blue shift of the extinction maximum of around 5 nm is observed and the onset of detectable extinction is blue-shifted significantly (Figure 1, **C4**).[64] Surprisingly, however, the reactivity is red-shifted and acrylamidylpyrene is reactive up to λ > 490 nm. While the reason for the red-shifted reactivity remains unclear, it is evident that, solely on the basis of UV/vis data, a prediction of the red shift in the experimentally observed reactivity would have been impossible. Importantly, the shift in activation wavelength was sufficient to

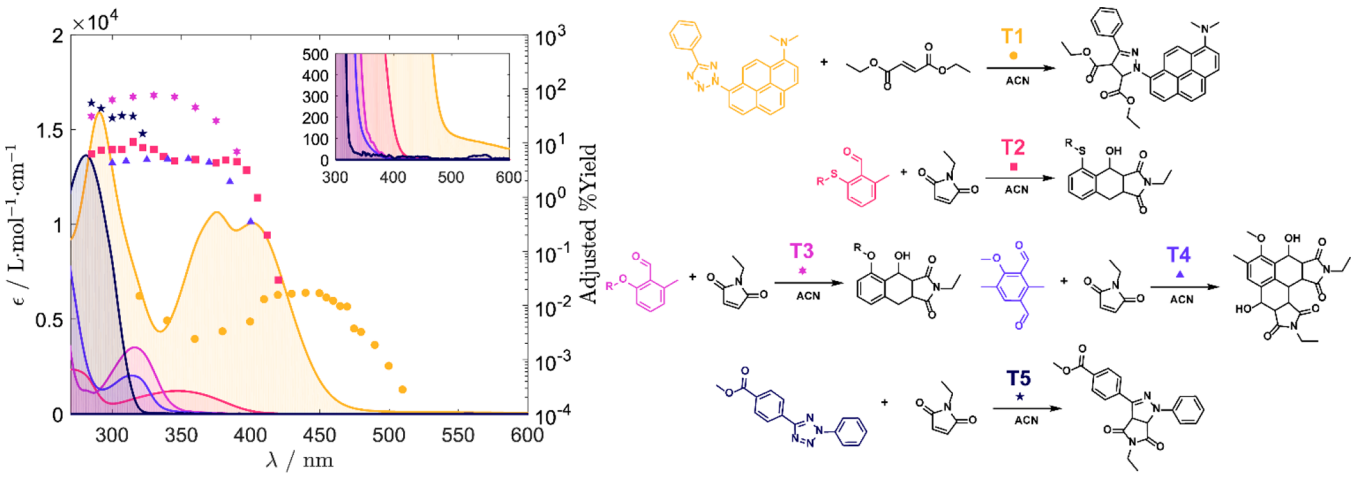

Figure 2. Molar extinction spectra (solid curves, left axis) and adjusted action plot yields (symbols, right axis) of various photothermal cascade reactions. For ease of comparison, percentage yields were adapted from the literature[72,78,79,81,82] and normalized by the number of photoreactive units in solution and the number of photons delivered to the sample to give adjusted % yields. The inset highlights the region of low absorption. For the full methodology to arrive at the displayed action plots, refer to the Supporting Information.

trigger acrylamidylpyrene dimerization selectively with λ_{max} = 455 nm centered LEDs in the presence of styrylpyrene. In the case of a pyrene-substituted chalcone, both the absorption maximum (λ_{max} = 415 nm) and the extinction onset are significantly red shifted in comparison to styrylpyrene (Figure 1, **C2**).[67] The peak reactivity was observed at λ = 440 nm, and reactivity was observed up to λ < 500 nm.

As outlined above, most synthetic attempts aim at substituting the phenyl ring of styrylpyrene. However, replacing the pyrene substituent with quinoxaline afforded a drastically red shifted stilbene derivative: i.e., styrylquinoxaline (λ_{max} = 380 nm in ACN; Figure 1, **C3**). During the investigation of the photophysical properties of styrylquinoxaline-terminated PEG, a slightly solvent dependent red shift (5 nm from ACN to H_2O) was observed. Remarkably, the solvent-dependent shift in reactivity was around 10 times more pronounced (50 nm from ACN to H_2O). In H_2O, the cycloaddition can be triggered with light of up to λ < 550 nm, making it the longest wavelength that can trigger catalyst-free photocycloadditions in solution to date. Furthermore, the reactivity of styrylquinoxaline can be turned off by protonating the slightly basic amines in acidic media, providing an additional level of reaction control.

Photochemical–Thermal Cascades. In addition to the purely photochemically driven cycloadditions, photochemical action plots have also been utilized to map the wavelength-dependent reactivity of a specific photochemical step involved within a larger cascade of reactions. In these examples, action plots report the yield of the final product formation as a function of wavelength, with no differentiation made between the yields of photoinduced and thermal events. Consequently, there may be an influence on the rate from subsequent thermal reactions. However, in most examples, the reaction partner (ene) is employed in large excess to ensure that the concentration of the ene is not rate-limiting. The photochemical–thermal cascades that have been mapped via wavelength-dependent action plots are based around two main classes of functionalities. The first is *o*-methylbenzaldehyde, which upon irradiation undergoes photoisomerization to yield an *o*-quinodimethane, an activated diene that readily reacts in a Diels–Alder [4 + 2] cycloaddition.[70] The second is 1,4-diaryltetrazole, which eliminates molecular nitrogen from the molecule after photoexcitation, affording a nitrile imine. When formed in the presence of a suitable dipolarophile, this reactive intermediate will undergo a 1,3-dipolar cycloaddition to yield a pyrazoline product.[71]

While both of these cascades have been employed in small-molecule syntheses and macromolecular ligation for a decade or more prior, they have always been induced by broad-band UV lamps. With the appeal of milder energy activation as a motivation, an action plot was employed to establish how much reactivity was accessible at these longer wavelengths. Both reactions proceeded with remarkably high efficiency after the initial excitation with suitable wavelengths.

o-Methylbenzaldehydes can be excited into the second singlet excited state through a $\pi \rightarrow \pi^*$ transition in the λ = 300–345 nm regime or into the first excited singlet state by an n $\rightarrow \pi^*$ transition at longer wavelengths (λ = 360–390 nm; Figure 2, **T3**). Even in this region of relatively weak comparative absorbance to the $\pi \rightarrow \pi^*$ transition, the reaction product was still observed. However, the reactivity from the n $\rightarrow \pi^*$ transition was strongly wavelength dependent, in contrast to the $\pi \rightarrow \pi^*$ transition. Here, longer wavelengths are less efficient in terms of comparative conversion, on the basis of the required intersystem crossing from a singlet to a triplet state, which subsequently rearranges into the triplet (*E*)-enol. While this is not the active isomer for thermal cycloaddition, the singlet (*Z*)-photoenol is efficiently formed, allowing the Diels–Alder cycloaddition to proceed. In comparison, tetrazoles returned more conventional action plots, with the highest efficiency of the cycloadduct generation being observed at wavelengths close to the maximum of the tetrazole extinction spectrum, correlating with an excitation into the first excited singlet state with a subsequent intersystem crossing to the triplet surface, yielding the nitrogen elimination (Figure 2, **T5**).[72]

On the basis of the information from the action plots, it was possible to design bespoke molecules, which undergo similar reactions at longer (visible) wavelengths. For the *o*-methylbenzaldehyde derivatives (Figure 2, **T2–T4**), it has been well established that the presence of an electron-donating ether moiety *ortho* to the aldehyde gave enhanced enolization

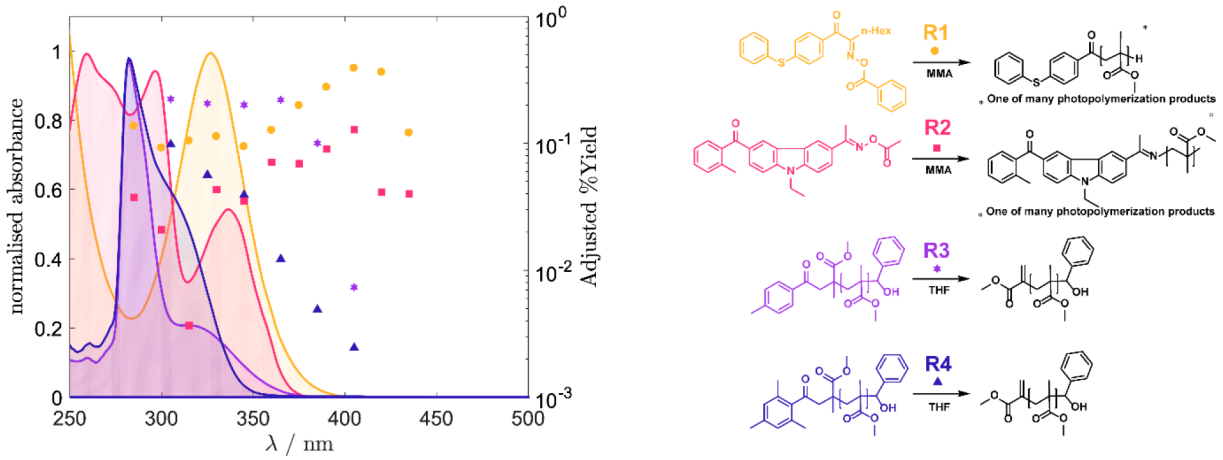

Figure 3. Normalized extinction spectra (solid curves, left axis) and adjusted action plot yield (symbols, right axis) of various photochemical release reactions for photoinitiation. For ease of comparison, percentage yields were adapted from the literature[5,80] and normalized by the number of photoreactive units in solution and the number of photons delivered to the sample to give adjusted % yields. For the full methodology to arrive at the displayed action plots, refer to the Supporting Information.

yields.[73] Replacing the ether with a thioether adduct resulted in two advantages.[74] First, it lowered the energy gap for the $\pi \rightarrow \pi^*$ transition that leads to the formation of the photoenol, subsequently red shifting the absorbance of the molecule. Second, the thioether moiety enforced and stabilized a favorable molecular conformation, enabling an enhanced excited-state intramolecular proton transfer. Indeed, an action plot investigation revealed a reactivity profile similar to that of the ether-substituted *o*-methylbenzaldehyde, but the wavelength where the maximum reactivity was observed was shifted by more than 40 nm (Figure 2, **T2**). Cycloaddition reactions were now possible in quantifiable amounts well into the visible regime, close to λ = 450 nm.[74]

A similar approach was employed for the tetrazole molecules; however, in this example, the N-aryl moiety was replaced with a larger polyaromatic group to yield a shift in the energy required to reach the first excited singlet state. The literature indicates that, while several moieties have been installed to effect a red-shifted absorbance (including substituted biphenyl,[75] thiophene,[76] and pyrenyl groups[77]), not all gave red-shifted cycloaddition reactivity. To date, the furthest that the photoinduced nitrile imine formation [3 + 2] cycloaddition has been pushed is when dual strategies of extending the conjugated system and introducing electron-donating substituents have been employed: specifically, a dimethylamino-functionalized pyrene as the N-aryl substituent (Figure 2, **T1**).[78] Action plot measurements of the dimethylamino pyrenyl aryl tetrazole demonstrated activity well into the green light regime at λ = 515 nm. Interestingly, this example, unlike the *N*-phenyl tetrazole, did not mirror the absorbance spectrum of the molecule, instead demonstrating an offset in reactivity by close to 25 nm. Again, this is slightly different from the *o*-methylbenzaldehyde example, as it appears to be not just the longer wavelength reactivity that is shifted but also the reactivity minima relative to the absorbance minima. Such behavior indicates that the photochemistry of the chromophore plays a role more critical than merely as an antenna for light absorbance.

One final example of a photochemical–thermal cascade is the photochemical release of a thioaldehyde from a pyreneacyl sulfide molecule.[79] Here, the photoexcited molecule eliminates the small molecule thioaldehyde, which is subsequently trapped by a nucleophile to yield an imine or oxime linkage, or a hetero-Diels–Alder reaction occurs to yield a sulfur-containing cycloadduct. Utilizing cyclopentadiene in excess as a trap, the action plot of this photorelease interestingly demonstrated a red-shifted photoreactivity in comparison with its absorbance spectrum (Figure 4, **R6**). However, the elimination occurs through a Norrish type II mechanism, correlating well with the trend of other Norrish-type photoelimination reactions discussed below.

Photochemical Release. While the reactivity of photocycloadditions has arguably been the most prevalent thus far, the very first action plot following our methodology was of a Norrish-type photorelease reaction published in 2017.[80] The photoreactivity of two commercial oxime-type photoinitiators, *O*-benzoyl-α-oxooxime (Figure 3, **R1**) and *O*-acetyloxime (Figure 3, **R2**) was investigated, prompted by the observation that the optimum wavelength for photochemically induced polymer formation did not seem to coincide with the absorption maximum.[80] The absorption maximum of *O*-benzoyl-α-oxooxime and *O*-acetyloxime is at approximately λ_{max} = 330 nm in ACN, correlating with the excitation of the N–O bond via n $\rightarrow \pi^*$ and $\pi \rightarrow \pi^*$ transitions, respectively. However, the most efficient wavelength for initiating the polymerization of acrylate type monomers was red-shifted by 75 nm relative to the absorbance maxima to λ = 405 nm,[80] where the molar extinction coefficients of **R1** and **R2** are 45 and 2.2 L mol^{-1} cm^{-1}, respectively. At the time, the discovery of the dissonance between the absorption maximum and the reaction maximum of a photoreactive moiety came as a surprise and prompted further investigation. To ensure that the results were not artifacts of side reactions due to high-intensity monochromatic laser light, the photopolymerizations were repeated with LEDs across the same wavelength range and the results were qualitatively congruent.

Building on our initial study, we carried out a second investigation into the photostability of photoinitiator-derived chain termini of polymers initiated by benzoyl-type fragments.[5] We investigated the Norrish-type I and II cleavages of the benzoyl chain end fragments of polymers at different wavelengths and found that the methyl substitution pattern of the benzoyl end group significantly affected its stability.[5] This study found that substitutions in the *ortho* position

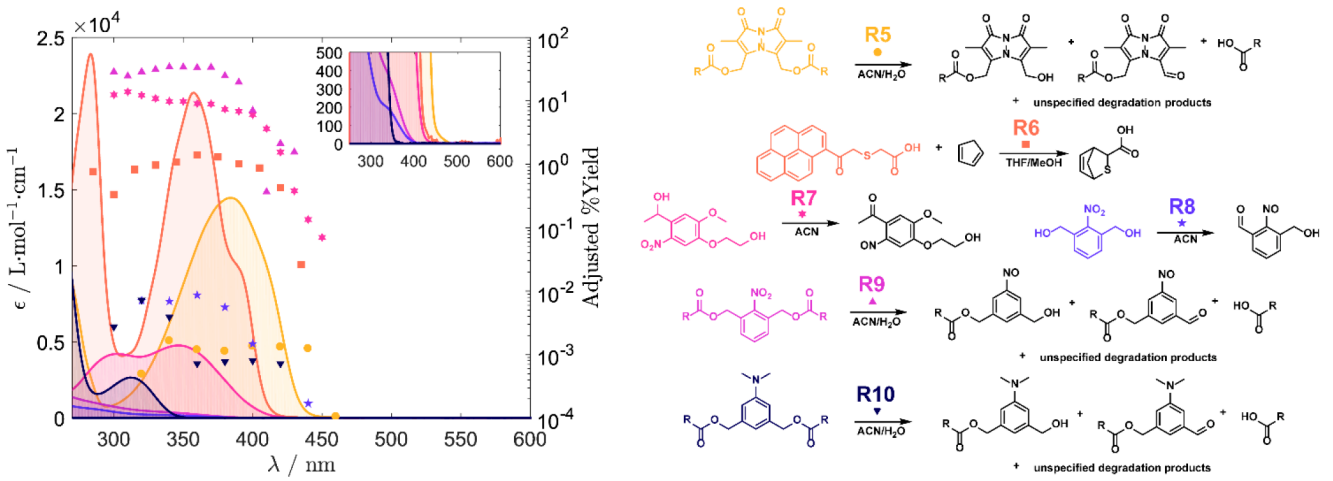

Figure 4. Molar extinction spectra (solid curves, left axis) and adjusted action plot yields (symbols, right axis) of various photochemical release reactions for photodegradation. For ease of comparison, percentage yields were adapted from the literature[87,88,90] and normalized by the number of photoreactive units in solution and the number of photons delivered to the sample to give adjusted % yields. The inset highlights the low-intensity absorption region. For the full methodology to arrive at the displayed action plots, refer to the Supporting Information.

resulted in the most substantial increase in the end-group stability. Further methyl substitution on the benzoyl group further increased the stability, although minutely. A direct comparison between the benzoyl chain termini with a single methyl substitution in the *para* position (Figure 3, **R3**) and three methyl substitutions filling the *para* and two *ortho* positions (Figure 3, **R4**) showed that **R4** was resistant to degradation under UV light up to λ = 345 nm and subsequently cleaved to form unsaturated species at a higher rate with shorter wavelengths. In contrast, **R3**, with the single *para*-substituted methyl group, already started cleaving at longer wavelengths of around λ = 385 nm, and then reached a plateau at around λ = 365 nm. According to DFT calculations, increasing the methyl substitution is likely to render increased inductive effects at the benzoyl moiety, resulting in changes to the HOMO and LUMO and shifting the activation energy to lower wavelengths.[5] As the stability of polymer coatings has been an issue that has fraught industry for a while, studies such as these, which focused on the photostability of initiator-derived end groups, helped to identify suitable initiators for specific applications.[83−86]

In addition to the exploration of Norrish-type reactions for photoinitiation, the photorelease of preformed polymer blocks and networks via Norrish pathways was also mapped. In two separate studies,[87,88] *o*-nitrobenzyl moieties were explored as potential photolytic units that could be incorporated into polymers to facilitate on-demand degradation. When the *o*-nitrobenzyl was modified by substituting two alcohol groups (Figure 4, **R8**) and an action plot was recorded, it was surprisingly found that the peak reactivity was only red-shifted by 10 nm relative to the absorption maximum (λ_{max} = 350 nm) associated with the N═O bond. However, the photorelease of the *o*-nitrobenzyl occurred at wavelengths up to λ < 425 nm, even when the absorption of the molecule appeared negligible beyond λ = 400 nm. This minor red shift of reactivity in comparison to the absorption maximum was also observed in the second study, targeting another *o*-nitrobenzyl species with one *ortho* position substituted with an isopropyl alcohol group and two alkoxy groups in the *meta* and *para* positions (Figure 4, **R7**).[88] Interestingly, the change of substituents at the *meta* and *para* positions seems to have resulted in a higher absorbance and reactivity in **R7**, in comparison to **R8**.

In the most recent study examining molecular photorelease properties via action plots, the wavelength-dependent photoreactivity of bimane, dimethylaminobenzene, and *o*-nitrobenzene thioether moieties (Figure 4, **R5**, **R9**, and **R10**, respectively) were explored. It is worth noting that the structures of **R8** and **R9** are identical, except for the substituents on the oxygen heteroatom, and their absorbances are comparable. Despite this, their reactivities were found to differ by 3 orders of magnitude (Figure 4). This is likely explained by the difference in the electron-donating effect between the substituents at the *ortho* positions of the phenyl ring, even if the substituent is three bond lengths away from the ring.[68,89] The above is further evidence for the notion that the absorption spectrum of a chromophore is not necessarily an accurate guide to its photoreactivity.

Through information afforded from the action plots, the molecules were designed in such a way that triggering the photorelease is achieved at independent wavelengths (going from visible to UV) in a hydrogel matrix via thiol−ene Michael additions.[90] While there are many established methods of controlling the mechanical properties of hydrogels, none of them afford the spatiotemporal control that light does.[91−96] The above study highlights the possibilities in the materials design space afforded by action plots, which we will explore in detail in the final part of the current Perspective.

In summary, a widely applied strategy to induce bathochromic absorption shifts of photoreactive molecules aims to lower the HOMO−LUMO gap in order to decrease the required energy for photochemical excitation.[97] This molecular engineering usually aims to lower the HOMO−LUMO gap through an extension of the π system and functionalization with electron-withdrawing and/or -donating groups. Such functionalization has been shown to induce the anticipated red shifts of absorbance and reactivity across a range of molecules; however, in other examples the photoreactivity was lost despite bathochromic absorption shifts.[75−77] Moreover, the effect of the substitution positions on the photoreactivity is largely unknown and should become the subject of future investigation via action plots.

While the implementation of action plots, as described in the current Perspective, has developed over the past 6 years, there is still immense unexplored potential for probing the limits of photoreactions. For example, solid-phase action plots or two-photon action plots are especially attractive for constructing photoresists for 3D laser lithography.[98] We acknowledge that the acquisition of a suitable pulsed, wavelength-tunable laser is likely the most significant impediment to action plots for monitoring covalent bond formation being more widely used in the scientific community. However, it is hoped that as the full potential of lasers and OPOs as photochemical tools is realized, they will become more in demand and therefore, hopefully, more accessible. So far, from nearly every reaction where the wavelength-dependent photoreactivity has been mapped, a red shift of the reactivity—relative to the absorption—has been observed, usually spanning across tens of nanometers. It is important to note that a similar red shift is observed in biological action spectra[22,99] and is often attributed to the variation in the transmission of different wavelengths through biological media. While that is clearly not the explanation here, we hypothesize that such an observation can be attributed to a combination of optical and chemical effects.

It was initially thought that the difference in optical penetration depth of short and long wavelengths may be the primary factor affecting reaction efficiency. However, applying Beer–Lambert's law to the example of the aforementioned two oxime photoinitiators (Figure 3, **R1** and **R2**) showed that the path lengths of the liquid samples would have to be greater than 2 cm for wavelengths longer than λ = 394 nm for **R1** and 381 nm for **R2** for 99% of the incident light to be absorbed in this specific case.[80] Similar calculations hold true for other systems where a strong red shift is observed.[72] Thus, the absorption profile alone cannot account for the significant discrepancy between absorption and conversion. Up to this point, we have assumed that the extinction has been entirely due to absorption processes; however, as mentioned above, this may not necessarily be the case. Scattering effects become more prominent as the ratio between particle size and irradiation wavelength approaches unity and thus will increase for shorter wavelengths. As a consequence, when extinction spectra alone are considered, the absorption may be overestimated in short-wavelength regions in lieu of scattering, contributing to the observed red shift.

From a more chemical perspective, the excited-state processes will play a key role in the wavelength-dependent reaction efficiency. In the cycloaddition examples noted above, it was suggested that the presence of conical intersections enabled efficient pathways to the formation of carbon-centered radicals at wavelengths above λ = 400 nm.[72,100] While this is supported by theoretical calculations, this explanation has yet to be empirically substantiated. Other mechanistic considerations involve π-orbital overlaps between chromophores, giving rise to transannular bands that serve as low-energy excited states. Upon thermal relaxation from this transannular state, the singlet excimer state of 9,10-dimethylenebianthracene became accessible and was proven to be highly efficient for photoreactions, leading to higher quantum yields at longer wavelengths.[101]

At present, the cause for the red shift in reactivity, in comparison to the absorbance spectrum, is still conjecture. In collating the data for this Perspective, we have highlighted that this phenomenon is not unique to one system but is common to numerous reaction classes. We therefore call upon our colleagues in physical and theoretical chemistry to aid in explaining these observations.

Translation of Action Plot Analysis to Materials Science. The above exploration has demonstrated that establishing action plots for covalent bond-forming and bond-cleavage reactions provides valuable insights into the optimum activation wavelength for a specific photochemical process. In the following, we turn our attention to how this information can be exploited in the pursuit of soft-matter material design and highlight critical elements that are still required in order to exploit the full potential of action plot analysis.

Particularly in the realm of 3D printing via methods such as stereolithography (SLA)[102−105] or direct laser writing (DLW)/3D laser lithography,[106−109] printing 3D structures that consist of multiple materials is an outstanding challenge. As noted in the Introduction, it would be highly desirable if the user of a 3D printer would be able to select not only the geometry but also the material property. Only an action plot analysis can provide the required information to exploit wavelength orthogonality. Modern additive manufacturing not only encompasses the macroscopic scale, but is also applied more and more on the nano- and microscopic scale, largely enabled by 3D laser lithography exploiting two-photon absorption processes. While the two-photon absorption cross-section of photoinitiators has been routinely measured,[110] there are very few examples of two-photon action plots.[111,112] Intuitively, one would expect that a one-photon action plot should also apply to two-photon absorption as well, yet rare examples in the literature suggest that this may not be the case. Recording two-photon action plots is perhaps one of the most important challenges, as such action plots will directly inform the choice of reactive chromophores for multicolor wavelength orthogonal 3D laser lithography. This task, however, requires overcoming specific experimental challenges, with the most significant being the limited conversions generated in small irradiated volumes. Ideally, action plots should be quantified using sensitive online methods such as UV–vis and fluorescence.[112,113] Indirect methods, such as a minimum power threshold where polymerization was observed, have also been used.[111] However, these methods do not provide structural information and therefore are unable to discern whether the same products are generated under one- and two-photon excitations. To address this important consideration, flow setups can be employed to generate sufficient conversion for a structural analysis such as NMR spectroscopy. Alternatively, chain growth mechanisms, such as free radical polymerization, can be exploited to amplify each absorption event.[5]

In the context of biomaterials engineering, it is highly desirable to apply noninvasive cytocompatible chemistries, e.g. those that do not require additives (catalysts or initiators) and can be activated by visible light, for altering the cross-linking density of the substrates. The striking outcome of the action plot studies (the red shift in photoreactivity in comparison to the absorbance spectra of the chromophores) has inspired the use of long-wavelength (up to λ = 510 nm) visible light in triggering the photochemical changes with high coupling efficiency.[65,67,78]

It has already been noted above that action plots were utilized for the design of advanced hydrogel materials. By an analysis of the specific wavelengths at which covalent bond

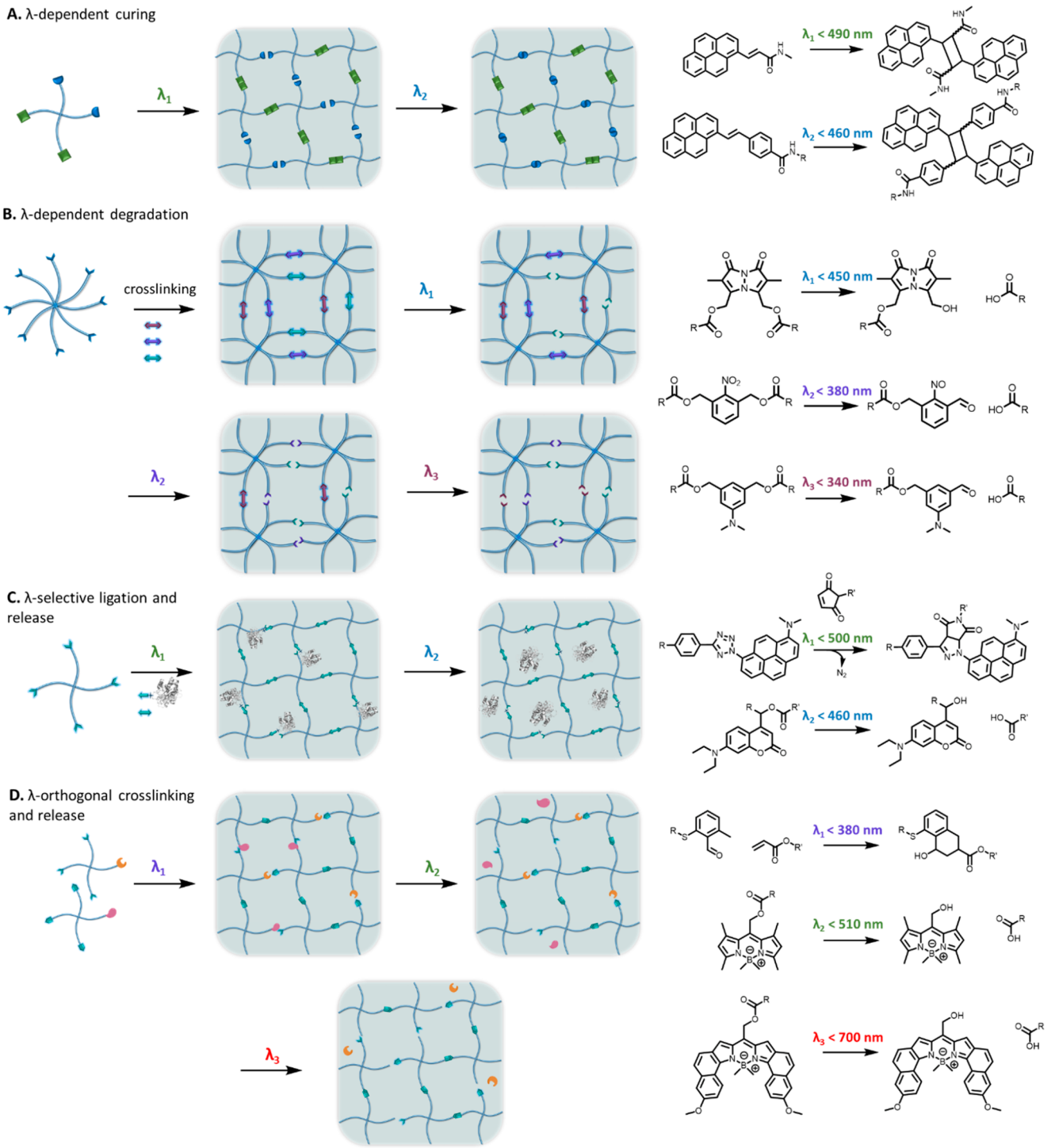

Figure 5. Selected material design concepts based on orthogonal photoactivatable functions by discrete colors of light that are enabled by action plot analyses. (A) Polymer network formation/photoresist curing by one wavelength (λ = 470 nm) and orthogonal curing of the structure by a different wavelength (λ = 440 nm). (B) Cleavage of a preformed material by blue light (λ = 420 nm), followed by UV (λ = 365 nm and subsequently 320 nm) light. (C) Conceptual design for cross-linking and tethering a biomolecule of interest by one wavelength (λ = 490 nm) followed by photorelease of the cargo using a different wavelength (λ = 440 nm). (D) Photocrosslinking of polymer chains (λ = 375 nm) featuring photolabile bioactive components that can be photouncaged by long wavelengths of visible light (λ = 480 and 680 nm). All phototriggered events are orthogonal to each other.

formation (or cleavage) is most efficient, it was possible to engineer hydrogel systems with precise elastic moduli, simply by irradiating with discrete colors of light (Figure 5A,B). The resulting technique for regulating the mechanics of hydrogels has significant implications for cell culture studies, where the cell behavior can be controlled through mild photoinduced mechanical cues. Specifically, multiple chromophores (i.e., styrylpyrene (**C5**) and acrylamidylpyrene (**C4**)) that can undergo [2 + 2] photocycloaddition have been incorporated into a four-arm poly(ethylene glycol) to enable selective cross-

linking of the polymer under irradiation at either λ = 455 or 420 nm.[64] The wavelength-selective stiffening triggers the detachment of fibroblasts cultured on the hydrogels, thus introducing a method for harvesting the cell sheets from the culture substrate using light.

More recently, three photocleavable moieties, bimane (**R5**), dimethylaminobenzene (**R9**), and oNB (**R10**) (Figure 4), were incorporated into hydrogel networks for wavelength-selective degradation of the materials. An analysis of the action plots on these chromophores revealed the wavelengths at which the photocleavage of each moiety could be accessed independently. Consequently, the hydrogels could be degraded in a stepwise fashion by exposure to light at λ = 420, 365, and 320 nm in that order, enabling the fabrication of hydrogels with user-defined storage moduli. When applied to a cell culture study, photoinduced softening of the hydrogels resulted in enhanced adhesion and spreading of preosteoblast cells on the cultured substrates.

In most systems developed to date, the activation sequence is wavelength-dependent: i.e., switching from green to blue to violet. With the help of action plots, it is possible to determine the required wavelengths to achieve orthogonal activation of independent photochemical events, such as photoligation and subsequent photodegradation, all within one polymer system (Figure 5C). Photochemically induced cross-linking of polymer chains in a wavelength-selective fashion—irrespective of the order in which the two different colors of light are applied—has been demonstrated in solution.[10] However, translating these findings to cured polymer networks is pivotal for designing cross-linked systems with desirable traits for advanced bioapplications. Wavelength-selective photoligation and photodegradation would allow the design of networks featuring bioactive components, such as proteins, to be phototethered to the polymer backbone using one wavelength, and the release of the cargo trigged by another wavelength. Ideally, both would be in the visible light regime. In addition to water-swollen hydrogel systems, such technology could be applied in the fabrication of photoresist scaffolds[114] for selective cell cultures, providing temporal release of different growth factors, all controlled by specific wavelengths of light, and enabling the formation of the organoids of interest in tissue engineering (Figure 5D).[115]

While the light-induced regulation of hydrogel properties has so far been demonstrated in bulk mechanics, such photochemical systems could also be applied in mask-based photolithography, for either photostiffened or photosoftened patterning of the material surfaces.[116] A longstanding challenge in this research area is the preparation of reproducible substrates with spatially resolved stiffness gradients, often attained using gradient photomasks or sliding masks to vary the light exposure.[117] Here, action plots can provide access to wavelength-selective photochemical activation, in order to facilitate the selective tuning of the substrate stiffness as a function of the color of light. In one example, poly(methyl methacrylate) and poly(4-vinylpyridine) polymers were functionalized with *o*-methylbenzaldehyde (**T3**, λ = 330 nm) and styrylpyrene (**C5**, λ = 435 nm) moieties, respectively, and the polymer blend was photocured with both colors of light to produce interpenetrating polymer networks.[118] This technique allowed the fabrication of surfaces with tunable, and spatially resolved, regions of disparate swelling ratios, using only a simple photomask.

While action plots are typically generated in solution with the aim to guide multicolor 3D printing and photochemical material design, it is perhaps even more attractive to map photochemical reactivity directly in quasi-solid-state systems such as hydrogels.[90] However, tracking chemical changes in networks is a formidable challenge that might be addressed using solid-state NMR techniques,[119−121] but more likely with a postirradiation analysis in specifically designed degradable networks, where the network fragments can be chemically analyzed.

CONCLUDING REMARKS

With regard to the recording of action plots, specific improvements are required that speak to the following processes. (i) The action plot data should be normalized to the number of absorbed photons, instead of depositing a constant number of photons at each wavelength. If the quantum yield is truly wavelength independent (as it should be across individual absorption bands), then such an experiment should result in a constant. Any deviation from such a trend at longer wavelengths could provide evidence toward resonance-enhanced intersystem crossing or temperature-dependent reaction quenching. We have made initial efforts to this effect on cycloaddition systems and the typical red shifts persist.[78] A challenge in these particular systems is the concentration required to observe dimerization, limiting light penetration through the sample. By attachment of the reactive chromophore as pendant groups on a polymer chain, and monitoring of the compaction due to folding, low concentrations and sufficient light penetration can be maintained, while proximity issues are eliminated. (ii) Recording action plots is currently mostly conducted off-line: i.e., the irradiated sample is analyzed postirradiation via NMR spectroscopy or liquid chromatography to quantify the conversion or yield. While in some cases it is possible to assess conversion via UV−vis or fluorescence spectroscopy, such as when the starting material and product have distinct optical features, this is not always feasible. In addition, these spectroscopic techniques do not allow for assessing the molecular structure of the formed products. An ideal tool for action plot mapping is the coupling of a tunable nanosecond laser system with an NMR spectrometer, directly feeding the light into the NMR probe head to enable the online monitoring of the molecular changes within a reaction mixture at distinct wavelengths. We note that the delivery of an exact quantifiable photon count to the sample within the probe head can be challenging. (iii) Methodologies need to be developed to record two-photon action plots. While measuring two-photon absorption cross sections is a routine procedure,[122] recording two-photon action plots—which is essential for advanced photoresists developed for 3D laser lithography—is not. The challenges lie in having a suitable wavelength-tunable femtosecond laser (noting that monochromaticity is lost to a large degree in a femtosecond laser pulse due to the Fourier principle) and the ability to irradiate sufficiently large sample volumes that allow the analysis of the generated products. We submit that overcoming the above three challenges is critical to further advance action-plot technology for bond-forming reactions to ultimately drive key material design outcomes, specifically in applications where wavelength orthogonality is of critical importance, including orthogonality to living systems. Finally, (iv), and perhaps most importantly, we note that theoreticians and experimentalists are called upon to devise approaches that

provide a mechanistic framework for understanding the observed red shifts, enabling us to provide a predictive framework for photochemical reactivity.

AUTHOR INFORMATION

Corresponding Authors

Christopher Barner-Kowollik − *School of Chemistry and Physics, Queensland University of Technology (QUT), Brisbane, Queensland 4000, Australia; Centre for Materials Science, Queensland University of Technology (QUT), Brisbane, Queensland 4000, Australia; Institute of Nanotechnology, Karlsruhe Institute of Technology (KIT), 76344 Eggenstein-Leopoldshafen, Germany;* orcid.org/0000-0002-6745-0570; Email: christopher.barnerkowollik@qut.edu.au, christopher.barner-kowollik@kit.edu

James P. Blinco − *School of Chemistry and Physics, Queensland University of Technology (QUT), Brisbane, Queensland 4000, Australia; Centre for Materials Science, Queensland University of Technology (QUT), Brisbane, Queensland 4000, Australia;* orcid.org/0000-0003-0092-2040; Email: j.blinco@qut.edu.au

Hendrik Frisch − *School of Chemistry and Physics, Queensland University of Technology (QUT), Brisbane, Queensland 4000, Australia; Centre for Materials Science, Queensland University of Technology (QUT), Brisbane, Queensland 4000, Australia;* orcid.org/0000-0001-8490-5082; Email: h.frisch@qut.edu.au

Vinh X. Truong − *School of Chemistry and Physics, Queensland University of Technology (QUT), Brisbane, Queensland 4000, Australia; Centre for Materials Science, Queensland University of Technology (QUT), Brisbane, Queensland 4000, Australia;* orcid.org/0000-0001-5553-6097; Email: vx.truong@qut.edu.au

Authors

Ishrath Mohamed Irshadeen − *School of Chemistry and Physics, Queensland University of Technology (QUT), Brisbane, Queensland 4000, Australia; Centre for Materials Science, Queensland University of Technology (QUT), Brisbane, Queensland 4000, Australia;* orcid.org/0000-0002-4823-7301

Sarah L. Walden − *School of Chemistry and Physics, Queensland University of Technology (QUT), Brisbane, Queensland 4000, Australia; Centre for Materials Science, Queensland University of Technology (QUT), Brisbane, Queensland 4000, Australia;* orcid.org/0000-0002-7625-4010

Martin Wegener − *Institute of Nanotechnology, Karlsruhe Institute of Technology (KIT), 76344 Eggenstein-Leopoldshafen, Germany*

Author Contributions

[‖]I.M.I and S.L.W. contributed equally.

Author Contributions

All authors contributed to the writing, editing, and formatting of the manuscript. All authors have given approval to the final version of the manuscript.

Notes

The authors declare no competing financial interest.

ACKNOWLEDGMENTS

C.B.-K. acknowledges funding from the Australian Research Council (ARC) in the form of a Laureate Fellowship (FL170100014) enabling his photochemical research program as well as continued key support from the Queensland University of Technology (QUT). C.B.-K., J.P.B., and M.W. acknowledge additional support via an ARC Discovery grant targeted at red-shifting photoligation chemistry. I.M.I. gratefully acknowledges QUT for a Ph.D. Research Scholarship. H.F. acknowledges support by the ARC in the form of a DECRA Fellowship DE200101096). M.W. and C.B.-K. acknowledge additional funding by the Deutsche Forschungsgemeinschaft (DFG, German Research Foundation) under Germany's Excellence Strategy for the Excellence Cluster "3D Matter Made to Order" (EXC-2082/1-390761711), by the Carl Zeiss Foundation, and by the Helmholtz program "Materials Systems Engineering". The authors thank Prof. Andreas Unterreiner (KIT) for helpful discussions during the revision process of this article.

REFERENCES

(1) Ciamician, G. The Photochemistry of The Future. *Science* **1912**, *36* (926), 385.

(2) Croce, R.; van Amerongen, H. Natural strategies for photosynthetic light harvesting. *Nat. Chem. Biol.* **2014**, *10* (7), 492−501.

(3) Hackett, P. A. Making Light Work—Applications of Lasers to Chemical Production. *Laser Chem.* **1988**, *9*, 75.

(4) Jablonski, A. Efficiency of Anti-Stokes Fluorescence in Dyes. *Nature* **1933**, *131* (3319), 839−840.

(5) Lauer, A.; Fast, D. E.; Steinkoenig, J.; Kelterer, A.-M.; Gescheidt, G.; Barner-Kowollik, C. Wavelength-Dependent Photochemical Stability of Photoinitiator-Derived Macromolecular Chain Termini. *ACS Macro Lett.* **2017**, *6* (9), 952−958.

(6) Demchenko, A. P.; Tomin, V. I.; Chou, P.-T. Breaking the Kasha Rule for More Efficient Photochemistry. *Chem. Rev.* **2017**, *117* (21), 13353−13381.

(7) Fan, X.; Chung, J. Y.; Lim, Y. X.; Li, Z.; Loh, X. J. Review of Adaptive Programmable Materials and Their Bioapplications. *ACS Appl. Mater. Interfaces* **2016**, *8* (49), 33351−33370.

(8) Yang, L.; Mayer, F.; Bunz, U. H. F.; Blasco, E.; Wegener, M. Multi-material multi-photon 3D laser micro- and nanoprinting. *Light: Advanced Manufacturing* **2021**, *2*, 1−17.

(9) Ligon-Auer, S. C.; Schwentenwein, M.; Gorsche, C.; Stampfl, J.; Liska, R. Toughening of photo-curable polymer networks: a review. *Polym. Chem.* **2016**, *7* (2), 257−286.

(10) Bialas, S.; Michalek, L.; Marschner, D. E.; Krappitz, T.; Wegener, M.; Blinco, J.; Blasco, E.; Frisch, H.; Barner-Kowollik, C. Access to Disparate Soft Matter Materials by Curing with Two Colors of Light. *Adv. Mater.* **2019**, *31* (8), 1807288.

(11) Bochet, C. G. Two Decades of Chromatic Orthogonality. *Isr. J. Chem.* **2021**, *61* (7−8), 486−495.

(12) Frisch, H.; Bloesser, F. R.; Barner-Kowollik, C. Controlling Chain Coupling and Single-Chain Ligation by Two Colours of Visible Light. *Angew. Chem., Int. Ed.* **2019**, *58* (11), 3604−3609.

(13) Neuman, K. C.; Chadd, E. H.; Liou, G. F.; Bergman, K.; Block, S. M. Characterization of Photodamage to Escherichia coli in Optical Traps. *Biophys. J.* **1999**, *77* (5), 2856−2863.
(14) MacLaughlin, J. A.; Anderson, R. R.; Holick, M. F. Spectral character of sunlight modulates photosynthesis of previtamin D3 and its photoisomers in human skin. *Science* **1982**, *216* (4549), 1001.
(15) Norval, M.; Björn, L. O.; de Gruijl, F. R. Is the action spectrum for the UV-induced production of previtamin D3 in human skin correct? *Photochemical & Photobiological Sciences* **2010**, *9* (1), 11−17.
(16) Schmalwieser, A. W.; Wallisch, S.; Diffey, B. A library of action spectra for erythema and pigmentation. *Photochemical & Photobiological Sciences* **2012**, *11* (2), 251−268.
(17) Setlow, R. B.; Setlow, J. K. Effects of Radiation on Polynucleotides. *Annu. Rev. Biophys. Bioeng.* **1972**, *1* (1), 293−346.
(18) Wikonkal, N. M.; Brash, D. E. Ultraviolet Radiation Induced Signature Mutations in Photocarcinogenesis. *J. Invest. Dermatol. Symp. Proc.* **1999**, *4* (1), 6−10.
(19) Freeman, S. E.; Hacham, H.; Gange, R. W.; Maytum, D. J.; Sutherland, J. C.; Sutherland, B. M. Wavelength dependence of pyrimidine dimer formation in DNA of human skin irradiated in situ with ultraviolet light. *Proc. Natl. Acad. Sci. U. S. A.* **1989**, *86* (14), 5605.
(20) de Gruijl, F. R.; Sterenborg, H. J.; Forbes, P. D.; Davies, R. E.; Cole, C.; Kelfkens, G.; van Weelden, H.; Slaper, H.; van der Leun, J. C. Wavelength dependence of skin cancer induction by ultraviolet irradiation of albino hairless mice. *Cancer Res.* **1993**, *53* (1), 53−60.
(21) Daubeny, C. On the Action of Light upon Plants, and of Plants upon the Atmosphere. *Philosophical Transactions of the Royal Society of London* **1836**, *126*, 149−175.
(22) Gates, F. L. A Study of The Bactericidal Aaction Of Ultra Violet Light: III. The Absorption of Ultra Violet Light by Bacteria. *J. Gen. Physiol.* **1930**, *14* (1), 31−42.
(23) Setlow, R. B.; Grist, E.; Thompson, K.; Woodhead, A. D. Wavelengths effective in induction of malignant melanoma. *Proc. Natl. Acad. Sci. U. S. A.* **1993**, *90* (14), 6666.
(24) Anderson, R. R.; Parrish, J. A. The Optics of Human Skin. *J. Invest. Dermatol.* **1981**, *77* (1), 13−19.
(25) Brainard, G. C.; Hanifin, J. P.; Greeson, J. M.; Byrne, B.; Glickman, G.; Gerner, E.; Rollag, M. D. Action Spectrum for Melatonin Regulation in Humans: Evidence for a Novel Circadian Photoreceptor. *J. Neurosci.* **2001**, *21* (16), 6405.
(26) Setlow, R. Action spectroscopy. *Adv. Biol. Med. Phys.* **1957**, *5*, 37−74.
(27) Coohill, T. P. Action Spectra Again?*. *Photochem. Photobiol.* **1991**, *54* (5), 859−870.
(28) Melchionna, M.; Fornasiero, P. Updates on the Roadmap for Photocatalysis. *ACS Catal.* **2020**, *10* (10), 5493−5501.
(29) Nayak, P. K.; Mahesh, S.; Snaith, H. J.; Cahen, D. Photovoltaic solar cell technologies: analysing the state of the art. *Nature Reviews Materials* **2019**, *4* (4), 269−285.
(30) Pettersson, L. A. A.; Roman, L. S.; Inganäs, O. Modeling photocurrent action spectra of photovoltaic devices based on organic thin films. *J. Appl. Phys.* **1999**, *86* (1), 487−496.
(31) Terao, Y.; Sasabe, H.; Adachi, C. Correlation of hole mobility, exciton diffusion length, and solar cell characteristics in phthalocyanine/fullerene organic solar cells. *Appl. Phys. Lett.* **2007**, *90* (10), 103515.
(32) Cushing, S. K.; Li, J.; Meng, F.; Senty, T. R.; Suri, S.; Zhi, M.; Li, M.; Bristow, A. D.; Wu, N. Photocatalytic Activity Enhanced by Plasmonic Resonant Energy Transfer from Metal to Semiconductor. *J. Am. Chem. Soc.* **2012**, *134* (36), 15033−15041.
(33) Kuang, D.; Uchida, S.; Humphry-Baker, R.; Zakeeruddin, S. M.; Grätzel, M. Organic Dye-Sensitized Ionic Liquid Based Solar Cells: Remarkable Enhancement in Performance through Molecular Design of Indoline Sensitizers. *Angew. Chem., Int. Ed.* **2008**, *47* (10), 1923−1927.
(34) Yoo, S.; Domercq, B.; Kippelen, B. Efficient thin-film organic solar cells based on pentacene/C60 heterojunctions. *Appl. Phys. Lett.* **2004**, *85* (22), 5427−5429.
(35) Wang, Z.-S.; Kawauchi, H.; Kashima, T.; Arakawa, H. Significant influence of TiO2 photoelectrode morphology on the energy conversion efficiency of N719 dye-sensitized solar cell. *Coord. Chem. Rev.* **2004**, *248* (13), 1381−1389.
(36) Sun, B.; Snaith, H. J.; Dhoot, A. S.; Westenhoff, S.; Greenham, N. C. Vertically segregated hybrid blends for photovoltaic devices with improved efficiency. *J. Appl. Phys.* **2005**, *97* (1), 014914.
(37) Ghosh, A. K.; Morel, D. L.; Feng, T.; Shaw, R. F.; Rowe, C. A. Photovoltaic and rectification properties of Al/Mg phthalocyanine/Ag Schottky-barrier cells. *J. Appl. Phys.* **1974**, *45* (1), 230−236.
(38) Thompson, B. C.; Kim, Y.-G.; Reynolds, J. R. Spectral Broadening in MEH-PPV:PCBM-Based Photovoltaic Devices via Blending with a Narrow Band Gap Cyanovinylene-Dioxythiophene Polymer. *Macromolecules* **2005**, *38* (13), 5359−5362.
(39) Gregg, B. A.; Fox, M. A.; Bard, A. J. Photovoltaic effect in symmetrical cells of a liquid crystal porphyrin. *J. Phys. Chem.* **1990**, *94* (4), 1586−1598.
(40) Dunbar, R. C.; Teng, H. H. I.; Fu, E. W. Photodissociation spectroscopy of halogen-substituted benzene ions. *J. Am. Chem. Soc.* **1979**, *101* (22), 6506−6510.
(41) Polfer, N.; Dugourd, P. *Laser Photodissociation and Spectroscopy of Mass-separated Biomolecular Ions*, 1st ed.; Springer: 2013; pp XI, 119.
(42) Uleanya, K. O.; Dessent, C. E. H. Investigating the mapping of chromophore excitations onto the electron detachment spectrum: photodissociation spectroscopy of iodide ion-thiouracil clusters. *Phys. Chem. Chem. Phys.* **2021**, *23* (2), 1021−1030.
(43) Cabré, G.; Garrido-Charles, A.; Moreno, M.; Bosch, M.; Porta-de-La-Riva, M.; Krieg, M.; Gascón-Moya, M.; Camarero, N.; Gelabert, R.; Lluch, J. M.; Busqué, F.; Hernando, J.; Gorostiza, P.; Alibés, R. Rationally designed azobenzene photoswitches for efficient two-photon neuronal excitation. *Nat. Commun.* **2019**, *10* (1), 907.
(44) Jacovella, U.; Carrascosa, E.; Buntine, J. T.; Ree, N.; Mikkelsen, K. V.; Jevric, M.; Moth-Poulsen, K.; Bieske, E. J. Photo- and Collision-Induced Isomerization of a Charge-Tagged Norbornadiene-Quadricyclane System. *J. Phys. Chem. Lett.* **2020**, *11* (15), 6045−6050.
(45) Marlton, S. J. P.; McKinnon, B. I.; Ucur, B.; Bezzina, J. P.; Blanksby, S. J.; Trevitt, A. J. Discrimination between Protonation Isomers of Quinazoline by Ion Mobility and UV-Photodissociation Action Spectroscopy. *J. Phys. Chem. Lett.* **2020**, *11* (10), 4226−4231.
(46) Wellman, S. M. J.; Jockusch, R. A. Moving in on the Action: An Experimental Comparison of Fluorescence Excitation and Photodissociation Action Spectroscopy. *J. Phys. Chem. A* **2015**, *119* (24), 6333−6338.
(47) Wellman, S. M. J.; Jockusch, R. A. Tuning the Intrinsic Photophysical Properties of Chlorophyll a. *Chem. - Eur. J.* **2017**, *23* (32), 7728−7736.
(48) Andrady, A. L., Wavelength sensitivity in polymer photodegradation. In *Polymer Analysis Polymer Physics*; Springer Berlin Heidelberg: 1997; pp 47−94.
(49) Liu, Y.; Wu, Z.; Kuhlenbeck, H.; Freund, H. J. Surface Action Spectroscopy: A Review and a Perspective on a New Technique to Study Vibrations at Surfaces. *Chem. Rec.* **2020**, *21* (6), 1270−1283.
(50) Karu, T. I.; Kolyakov, S. F. Exact Action Spectra for Cellular Responses Relevant to Phototherapy. *Photomed. Laser Surg.* **2005**, *23* (4), 355−361.
(51) Bohren, C. F.; Huffman, D. R. *Absorption and scattering of light by small particles*; Wiley: 2008.
(52) He, Q.; Fang, Z.; Shoshamin, O.; Brown, S. S.; Rudich, Y. Scattering and Absorption Cross-sections of Atmospheric Gases in the Ultraviolet-Visible Wavelength Range (307−725 nm). *Atmos. Chem. Phys.* **2021**, *21*, 14927−14940.
(53) Fritzsche. Ueber die festen Kohlenwasserstoffe des Steinkohlentheers. *J. Prakt. Chem.* **1867**, *101* (1), 333−343.
(54) Zdobinsky, T.; Sankar Maiti, P.; Klajn, R. Support Curvature and Conformational Freedom Control Chemical Reactivity of Immobilized Species. *J. Am. Chem. Soc.* **2014**, *136* (7), 2711−2714.
(55) Ihara, T.; Fujii, T.; Mukae, M.; Kitamura, Y.; Jyo, A. Photochemical Ligation of DNA Conjugates through Anthracene

Cyclodimer Formation and Its Fidelity to the Template Sequences. *J. Am. Chem. Soc.* **2004**, *126* (29), 8880−8881.
(56) Chen, X.-Y.; Chen, H.; Đorđevisć, L.; Guo, Q.-H.; Wu, H.; Wang, Y.; Zhang, L.; Jiao, Y.; Cai, K.; Chen, H.; Stern, C. L.; Stupp, S. I.; Snurr, R. Q.; Shen, D.; Stoddart, J. F. Selective Photodimerization in a Cyclodextrin Metal-Organic Framework. *J. Am. Chem. Soc.* **2021**, *143* (24), 9129−9139.
(57) Yamamoto, T.; Yagyu, S.; Tezuka, Y. Light- and Heat-Triggered Reversible Linear-Cyclic Topological Conversion of Telechelic Polymers with Anthryl End Groups. *J. Am. Chem. Soc.* **2016**, *138* (11), 3904−3911.
(58) Kislyak, A.; Frisch, H.; Gernhardt, M.; Van Steenberge, P. H. M.; D'Hooge, D. R.; Barner-Kowollik, C. Time-Dependent Differential and Integral Quantum Yields for Wavelength-Dependent [4 + 4] Photocycloadditions. *Chem. - Eur. J.* **2020**, *26* (2), 478−484.
(59) Kislyak, A.; Kodura, D.; Frisch, H.; Feist, F.; Van Steenberge, P. H. M.; Barner-Kowollik, C.; D'Hooge, D. R. A holistic approach for anthracene photochemistry kinetics. *Chem. Eng. J.* **2020**, *402*, 126259.
(60) Doi, T.; Kawai, H.; Murayama, K.; Kashida, H.; Asanuma, H. Visible-Light-Triggered Cross-Linking of DNA Duplexes by Reversible [2 + 2] Photocycloaddition of Styrylpyrene. *Chem. - Eur. J.* **2016**, *22* (30), 10533−10538.
(61) Kovalenko, N. P.; Abdukadirov, A.; Gerko, V. I.; Alfimov, M. V. Some peculiarities of diarylethylenes with 3-pyrenyl fragments. *J. Appl. Spectrosc.* **1980**, *32* (6), 607−612.
(62) Frisch, H.; Menzel, J. P.; Bloesser, F. R.; Marschner, D. E.; Mundsinger, K.; Barner-Kowollik, C. Photochemistry in Confined Environments for Single-Chain Nanoparticle Design. *J. Am. Chem. Soc.* **2018**, *140* (30), 9551−9557.
(63) Marschner, D. E.; Frisch, H.; Offenloch, J. T.; Tuten, B. T.; Becer, C. R.; Walther, A.; Goldmann, A. S.; Tzvetkova, P.; Barner-Kowollik, C. Visible Light [2 + 2] Cycloadditions for Reversible Polymer Ligation. *Macromolecules* **2018**, *51* (10), 3802−3807.
(64) Kalayci, K.; Frisch, H.; Barner-Kowollik, C.; Truong, V. X. Wavelength-Dependent Stiffening of Hydrogel Matrices via Red-shifted [2 + 2] Photocycloadditions. *Adv. Funct. Mater.* **2020**, *30* (15), 1908171.
(65) Kalayci, K.; Frisch, H.; Truong, V. X.; Barner-Kowollik, C. Green light triggered [2 + 2] cycloaddition of halochromic styrylquinoxaline—controlling photoreactivity by pH. *Nat. Commun.* **2020**, *11* (1), 4193.
(66) Marschner, D. E.; Kamm, P. W.; Frisch, H.; Unterreiner, A.-N.; Barner-Kowollik, C. Photocycloadditions in disparate chemical environments. *Chem. Commun.* **2020**, *56* (90), 14043−14046.
(67) Irshadeen, I. M.; De Bruycker, K.; Micallef, A. S.; Walden, S. L.; Frisch, H.; Barner-Kowollik, C. Green light LED activated ligation of a scalable, versatile chalcone chromophore. *Polym. Chem.* **2021**, *12* (34), 4903−4909.
(68) Hansen, M. J.; Velema, W. A.; Lerch, M. M.; Szymanski, W.; Feringa, B. L. Wavelength-selective cleavage of photoprotecting groups: strategies and applications in dynamic systems. *Chem. Soc. Rev.* **2015**, *44* (11), 3358−3377.
(69) Ludwanowski, S.; Hoenders, D.; Kalayci, K.; Frisch, H.; Barner-Kowollik, C.; Walther, A. Modular functionalization and hydrogel formation via red-shifted and self-reporting [2 + 2] cycloadditions. *Chem. Commun.* **2021**, *57* (6), 805−808.
(70) Gruendling, T.; Oehlenschlaeger, K. K.; Frick, E.; Glassner, M.; Schmid, C.; Barner-Kowollik, C. Rapid UV Light-Triggered Macromolecular Click Conjugations via the Use of o-Quinodimethanes. *Macromol. Rapid Commun.* **2011**, *32* (11), 807−812.
(71) Dietrich, M.; Delaittre, G.; Blinco, J. P.; Inglis, A. J.; Bruns, M.; Barner-Kowollik, C. Photoclickable Surfaces for Profluorescent Covalent Polymer Coatings. *Adv. Funct. Mater.* **2012**, *22* (2), 304−312.
(72) Menzel, J. P.; Noble, B. B.; Lauer, A.; Coote, M. L.; Blinco, J. P.; Barner-Kowollik, C. Wavelength Dependence of Light-Induced Cycloadditions. *J. Am. Chem. Soc.* **2017**, *139* (44), 15812−15820.
(73) Pauloehrl, T.; Delaittre, G.; Winkler, V.; Welle, A.; Bruns, M.; Börner, H. G.; Greiner, A. M.; Bastmeyer, M.; Barner-Kowollik, C. Adding Spatial Control to Click Chemistry: Phototriggered Diels-Alder Surface (Bio)functionalization at Ambient Temperature. *Angew. Chem., Int. Ed.* **2012**, *51* (4), 1071−1074.
(74) Feist, F.; Menzel, J. P.; Weil, T.; Blinco, J. P.; Barner-Kowollik, C. Visible Light-Induced Ligation via o-Quinodimethane Thioethers. *J. Am. Chem. Soc.* **2018**, *140* (37), 11848−11854.
(75) Blasco, E.; Sugawara, Y.; Lederhose, P.; Blinco, J. P.; Kelterer, A.-M.; Barner-Kowollik, C. Understanding Reactivity Patterns in Light-Induced Nitrile Imine Mediated Tetrazole-Ene Cycloadditions. *ChemPhotoChem.* **2017**, *1* (5), 159−163.
(76) An, P.; Yu, Z.; Lin, Q. Design of oligothiophene-based tetrazoles for laser-triggered photoclick chemistry in living cells. *Chem. Commun.* **2013**, *49* (85), 9920−9922.
(77) Lederhose, P.; Wüst, K. N. R.; Barner-Kowollik, C.; Blinco, J. P. Catalyst free visible light induced cycloaddition as an avenue for polymer ligation. *Chem. Commun.* **2016**, *52* (35), 5928−5931.
(78) Kamm, P. W.; Blinco, J. P.; Unterreiner, A.-N.; Barner-Kowollik, C. Green-light induced cycloadditions. *Chem. Commun.* **2021**, *57* (33), 3991−3994.
(79) Tuten, B. T.; Menzel, J. P.; Pahnke, K.; Blinco, J. P.; Barner-Kowollik, C. Pyreneacyl sulfides as a visible light-induced versatile ligation platform. *Chem. Commun.* **2017**, *53* (32), 4501−4504.
(80) Fast, D. E.; Lauer, A.; Menzel, J. P.; Kelterer, A.-M.; Gescheidt, G.; Barner-Kowollik, C. Wavelength-Dependent Photochemistry of Oxime Ester Photoinitiators. *Macromolecules* **2017**, *50* (5), 1815−1823.
(81) Feist, F.; Walden, S. L.; Alves, J.; Kunz, S. V.; Micallef, A. S.; Brock, A. J.; McMurtrie, J. C.; Weil, T.; Blinco, J. P.; Barner-Kowollik, C. Wavelength-Gated Photochemical Synthesis of Phenalene Diimides. *Angew. Chem., Int. Ed.* **2021**, *60* (18), 10402−10408.
(82) Menzel, J. P.; Noble, B. B.; Blinco, J. P.; Barner-Kowollik, C. Predicting wavelength-dependent photochemical reactivity and selectivity. *Nat. Commun.* **2021**, *12* (1), 1691.
(83) Johnson, B. W.; McIntyre, R. Analysis of test methods for UV durability predictions of polymer coatings. *Prog. Org. Coat.* **1996**, *27* (1), 95−106.
(84) Gu, X.; Michaels, C. A.; Drzal, P. L.; Jasmin, J.; Martin, D.; Nguyen, T.; Martin, J. W. Probing photodegradation beneath the surface: a depth profiling study of UV-degraded polymeric coatings with microchemical imaging and nanoindentation. *Journal of Coatings Technology and Research* **2007**, *4* (4), 389.
(85) Nguyen, T.; Martin, J.; Byrd, E.; Embree, N. Relating laboratory and outdoor exposure of coatingsIII. Effect of relative humidity on moisture-enhanced photolysis of acrylic-melamine coatings. *Polym. Degrad. Stab.* **2002**, *77* (1), 1−16.
(86) Yousif, E.; Haddad, R. Photodegradation and photostabilization of polymers, especially polystyrene: review. *SpringerPlus* **2013**, *2*, 398−398.
(87) Petit, C.; Bachmann, J.; Michalek, L.; Catel, Y.; Blasco, E.; Blinco, J. P.; Unterreiner, A.-N.; Barner-Kowollik, C. UV-induced photolysis of polyurethanes. *Chem. Commun.* **2021**, *57* (23), 2911−2914.
(88) Bachmann, J.; Petit, C.; Michalek, L.; Catel, Y.; Blasco, E.; Blinco, J. P.; Unterreiner, A.-N.; Barner-Kowollik, C. Chain-Length-Dependent Photolysis of ortho-Nitrobenzyl-Centered Polymers. *ACS Macro Lett.* **2021**, *10* (4), 447−452.
(89) Abou Nakad, E.; Bolze, F.; Specht, A. o-Nitrobenzyl photoremovable groups with fluorescence uncaging reporting properties. *Org. Biomol. Chem.* **2018**, *16* (33), 6115−6122.
(90) Pelloth, J. L.; Tran, P. A.; Walther, A.; Goldmann, A. S.; Frisch, H.; Truong, V. X.; Barner-Kowollik, C. Wavelength-Selective Softening of Hydrogel Networks. *Adv. Mater.* **2021**, *33* (39), No. 2102184.
(91) Zerobin, E.; Markovic, M.; Tomášiková, Z.; Qin, X.-H.; Ret, D.; Steinbauer, P.; Kitzmüller, J.; Steiger, W.; Gruber, P.; Ovsianikov, A.; Liska, R.; Baudis, S. Hyaluronic acid vinyl esters: A toolbox toward controlling mechanical properties of hydrogels for 3D microfabrication. *J. Polym. Sci.* **2020**, *58* (9), 1288−1298.

(92) Lee, K. Y.; Rowley, J. A.; Eiselt, P.; Moy, E. M.; Bouhadir, K. H.; Mooney, D. J. Controlling Mechanical and Swelling Properties of Alginate Hydrogels Independently by Cross-Linker Type and Cross-Linking Density. *Macromolecules* **2000**, *33* (11), 4291−4294.
(93) Cha, C.; Shin, S. R.; Gao, X.; Annabi, N.; Dokmeci, M. R.; Tang, X.; Khademhosseini, A. Controlling Mechanical Properties of Cell-Laden Hydrogels by Covalent Incorporation of Graphene Oxide. *Small* **2014**, *10* (3), 514−523.
(94) Wu, X.; Huang, W.; Wu, W.-H.; Xue, B.; Xiang, D.; Li, Y.; Qin, M.; Sun, F.; Wang, W.; Zhang, W.-B.; Cao, Y. Reversible hydrogels with tunable mechanical properties for optically controlling cell migration. *Nano Res.* **2018**, *11* (10), 5556−5565.
(95) Tse, J. R.; Engler, A. J. Preparation of Hydrogel Substrates with Tunable Mechanical Properties. *Current Protocols in Cell Biology* **2010**, *47* (1), 10.16.1−10.16.16.
(96) Xiang, D.; Wu, X.; Cao, W.; Xue, B.; Qin, M.; Cao, Y.; Wang, W. Hydrogels With Tunable Mechanical Properties Based on Photocleavable Proteins. *Front. Chem.* **2020**, *8* (7), 1.
(97) Bléger, D.; Hecht, S. Visible-Light-Activated Molecular Switches. *Angew. Chem., Int. Ed.* **2015**, *54* (39), 11338−11349.
(98) Bougdid, Y.; Sekkat, Z. Voxels Optimization in 3D Laser Nanoprinting. *Sci. Rep.* **2020**, *10* (1), 10409.
(99) Zhen, S.; Haidekker, M.; van Iersel, M. W. Far-red light enhances photochemical efficiency in a wavelength-dependent manner. *Physiol. Plant.* **2019**, *167* (1), 21−33.
(100) Worth, G. A.; Cederbaum, L. S. Beyond Born-Oppenheimer: Molecular Dynamics Through a Conical Intersection. *Annu. Rev. Phys. Chem.* **2004**, *55* (1), 127−158.
(101) Shizuka, H.; Ishii, Y.; Hoshino, M.; Morita, T. Wavelength-dependent photochemical behavior in 9,10-dimethylenebianthracene. *J. Phys. Chem.* **1976**, *80* (1), 30−32.
(102) Melchels, F. P. W.; Feijen, J.; Grijpma, D. W. A review on stereolithography and its applications in biomedical engineering. *Biomaterials* **2010**, *31* (24), 6121−6130.
(103) Huang, J. G.; Qin, Q.; Wang, J. A Review of Stereolithography: Processes and Systems. *Processes* **2020**, *8* (9), 1138.
(104) Halloran, J. W. Ceramic Stereolithography: Additive Manufacturing for Ceramics by Photopolymerization. *Annu. Rev. Mater. Res.* **2016**, *46* (1), 19−40.
(105) Manapat, J. Z.; Chen, Q.; Ye, P.; Advincula, R. C. 3D Printing of Polymer Nanocomposites via Stereolithography. *Macromol. Mater. Eng.* **2017**, *302* (9), 1600553.
(106) Selimis, A.; Mironov, V.; Farsari, M. Direct laser writing: Principles and materials for scaffold 3D printing. *Microelectron. Eng.* **2015**, *132*, 83−89.
(107) Belqat, M.; Wu, X.; Gomez, L. P. C.; Malval, J.-P.; Dominici, S.; Leuschel, B.; Spangenberg, A.; Mougin, K. Tuning nanomechanical properties of microstructures made by 3D direct laser writing. *Additive Manufacturing* **2021**, *47*, 102232.
(108) Anscombe, N. Direct laser writing. *Nat. Photonics* **2010**, *4* (1), 22−23.
(109) Barner-Kowollik, C.; Bastmeyer, M.; Blasco, E.; Delaittre, G.; Müller, P.; Richter, B.; Wegener, M. 3D Laser Micro- and Nanoprinting: Challenges for Chemistry. *Angew. Chem., Int. Ed.* **2017**, *56* (50), 15828−15845.
(110) Schafer, K. J.; Hales, J. M.; Balu, M.; Belfield, K. D.; Van Stryland, E. W.; Hagan, D. J. Two-photon absorption cross-sections of common photoinitiators. *J. Photochem. Photobiol., A* **2004**, *162* (2), 497−502.
(111) Baldacchini, T.; LaFratta, C. N.; Farrer, R. A.; Teich, M. C.; Saleh, B. E. A.; Naughton, M. J.; Fourkas, J. T. Acrylic-based resin with favorable properties for three-dimensional two-photon polymerization. *J. Appl. Phys.* **2004**, *95* (11), 6072−6076.
(112) Bozio, R.; Cecchetto, E.; Fabbrini, G.; Ferrante, C.; Maggini, M.; Menna, E.; Pedron, D.; Riccò, R.; Signorini, R.; Zerbetto, M. One- and Two-Photon Absorption and Emission Properties of a Zn(II) Chemosensor. *J. Phys. Chem. A* **2006**, *110* (20), 6459−6464.
(113) Su Lim, C.; Won Kang, D.; Shun Tian, Y.; Hee Han, J.; Lim Hwang, H.; Rae Cho, B. Detection of mercury in fish organs with a two-photon fluorescent probe. *Chem. Commun.* **2010**, *46* (14), 2388−2390.
(114) Richter, B.; Hahn, V.; Bertels, S.; Claus, T. K.; Wegener, M.; Delaittre, G.; Barner-Kowollik, C.; Bastmeyer, M. Guiding Cell Attachment in 3D Microscaffolds Selectively Functionalized with Two Distinct Adhesion Proteins. *Adv. Mater.* **2017**, *29* (5), 1604342.
(115) Hippler, M.; Lemma, E. D.; Bertels, S.; Blasco, E.; Barner-Kowollik, C.; Wegener, M.; Bastmeyer, M. 3D Scaffolds to Study Basic Cell Biology. *Adv. Mater.* **2019**, *31* (26), 1808110.
(116) Goldmann, A. S.; Boase, N. R. B.; Michalek, L.; Blinco, J. P.; Welle, A.; Barner-Kowollik, C. Adaptable and Reprogrammable Surfaces. *Adv. Mater.* **2019**, *31* (40), 1902665.
(117) Munoz-Robles, B. G.; Kopyeva, I.; DeForest, C. A. Surface Patterning of Hydrogel Biomaterials to Probe and Direct Cell-Matrix Interactions. *Adv. Mater. Interfaces* **2020**, *7* (21), 2001198.
(118) Michalek, L.; Bialas, S.; Walden, S. L.; Bloesser, F. R.; Frisch, H.; Barner-Kowollik, C. 2D Fabrication of Tunable Responsive Interpenetrating Polymer Networks from a Single Photoresist. *Adv. Funct. Mater.* **2020**, *30* (48), 2005328.
(119) Reif, B.; Ashbrook, S. E.; Emsley, L.; Hong, M. Solid-state NMR spectroscopy. *Nature Reviews Methods Primers* **2021**, *1* (1), 2.
(120) Ashbrook, S. E.; Griffin, J. M.; Johnston, K. E. Recent Advances in Solid-State Nuclear Magnetic Resonance Spectroscopy. *Annu. Rev. Anal. Chem.* **2018**, *11* (1), 485−508.
(121) El Hariri El Nokab, M.; van der Wel, P. C. A. Use of solid-state NMR spectroscopy for investigating polysaccharide-based hydrogels: A review. *Carbohydr. Polym.* **2020**, *240*, 116276.
(122) Sheik-Bahae, M.; Said, A. A.; Wei, T.; Hagan, D. J.; Stryland, E. W. V. Sensitive measurement of optical nonlinearities using a single beam. *IEEE J. Quantum Electron.* **1990**, *26* (4), 760−769.